Available online at www.sciencedirect.com
SCIENCE DIRECT®
ELSEVIER
International Journal of Solids and Structures 42 (2005) 3411–3437
INTERNATIONAL JOURNAL OF SOLIDS and STRUCTURES
www.elsevier.com/locate/ijsolstr

Analysis of an elastic ring tourniquet (ERT) using the theory of a Cosserat curve and finite elements

M.B. Rubin [a,*], E. Mazza [b]

[a] *Faculty of Mechanical Engineering, Technion-Israel Institute of Technology, 32000 Haifa, Israel*
[b] *Institute of Mechanical Systems, Department of Mechanical Engineering, ETH Zentrum, 8092 Zürich, Switzerland*

Received 5 May 2004; received in revised form 4 October 2004
Available online 15 December 2004

Abstract

A-TT™ and S-MART™ are novel elastic ring tourniquets (ERTs) used for the control of hemodynamic shock and for bloodless surgical procedures on limbs. The ERT device is essentially a silicone ring surrounded by a stockinette sterile gauze. Since the contact pressure applied by the ERT is determined by its geometric and mechanical properties and cannot be adjusted, it is important to develop a mechanical model that can be used to ensure that the contact pressure remains low enough not to cause local tissue damage. Although the calculation of the contact pressure applied by a silicone ring seems to be a simple classical problem, it is shown that the accurate prediction of this contact pressure requires analysis of a number of complicating features, which are related to nonlinear geometric and material influences. This paper presents a hierarchy of mechanical models which include: a simple strength of materials model; models based on the theory of a Cosserat curve and a generalized string (which includes deformation of the cross-section); exact axisymmetric plane strain nonlinear elasticity; and axisymmetric nonlinear finite element analysis. It is shown that the Cosserat model provides reasonable predictions of the response of the silicone ring. Since numerical simulations with the Cosserat model are much faster than those with the finite element model, the Cosserat analysis is more suitable for optimization of the thickness of the stockinette, which can significantly reduce both the maximum and average contact pressures applied by the ERT on the skin.

Keywords: Auto transfusion; Contact; Cosserat; Elastic ring; Tourniquet

* Corresponding author. Tel.: +972 4 829 3188; fax: +972 4 829 5711.
E-mail addresses: mbrubin@tx.technion.ac.il (M.B. Rubin), edoardo.mazza@imes.mavt.ethz.ch (E. Mazza).

0020-7683/$ - see front matter © 2004 Elsevier Ltd. All rights reserved.
doi:10.1016/j.ijsolstr.2004.10.034

1. Introduction

The problem of the contact pressure between an elastic ring and a rigid cylinder is the classical Lame problem in linear elasticity. The solution is relevant for shrink fittings and lubrication seals. However, the present work is motivated by a biomedical application where an elastic ring tourniquet (ERT) is used in emergency medicine to displace blood from the limbs for treatment of patients in hemodynamic shock or cardiac arrest. Although the analysis of the ERT seems to be simple, it is shown that the problem is actually quite complicated and requires examination of the influence of a number of nonstandard effects which include:

(E1) Modeling cross-sectional deformations in the ring,
(E2) Modeling the shape of the cross-section,
(E3) Large deformations,
(E4) Values of pressure which are not small relative to the circumferential stress,
(E5) Material nonlinearity,
(E6) Bending effects.

By way of background it is noted that the effect of the ERT is an Auto-Transfusion Tourniquet (A-TT™, OHK Medical Devices, 2002) which brings the patient's own blood into the vital organs. Another version of the ERT (S-MART™, OHK Medical Devices, 2002) is used in orthopedic surgery to remove the blood (exsanguinate) from a limb prior to and during surgery in order to create an essentially bloodless surgical field. Both devices apply constricting pressure on the limb to the extent that the arteries and other blood vessels within it are collapsed and blood ceases to flow into the limb.

The ERT device is essentially a toroidal ring of silicone which has a circular cross-section. A sterile elastic sleeve (stockinette) is rolled onto the ring together with ribbons and handles. By merely pulling the handles apart, the ring and stockinette roll onto the limb from the distal to the proximal ends and the mean radius of the ring is expanded to 1.5–2.5 times its unstressed value. The objective of applying the tourniquet is to temporarily totally occlude the blood vessels in the limb by increasing the pressure in the limb above the patient's systolic blood pressure. However, the pressure applied by the ERT on the tissue must be limited to ensure that the tissue is not damaged. Direct measurement of the pressure applied between a biomedical device and the compliant tissue is known to be quite difficult and special transducers have been developed for such applications (Paris-Seeley et al., 2000). Moreover, unlike for a standard pressure cuff, there is no gauge that monitors pressure. Specifically, the contact pressure applied by the S-MART™ device cannot be adjusted and is determined by the dimensions of the device and the dimensions of the limb. Consequently, it is important to develop a mechanical model which can predict the magnitude of this contact pressure.

During the development stages of the device a large number of experiments were performed on consenting human subjects to asses: the extent of blood vessel occlusion, the level of discomfort due to the pressure applied by the device, and to ensure that no tissue damage was observable. More recently, the device has been evaluated in a number of bloodless surgeries on the hand (Boiko and Roffman, 2004). The results of these clinical evaluations confirm the ease with which the device can be applied, its success in occluding the blood flow, reduced application time of the tourniquet, and the fact that no tissue damage was observed either during the operation or during post-operative follow-up examinations.

A complete analysis of the ERT would require a difficult finite element calculation which should include nonlinear geometric effects and accurate modeling of the constitutive properties of the silicone ring, the stockinette and the tissues in the limb. Such a complete analysis is outside of the scope of the present work, especially since the constitutive properties of the tissues in the limb are not known. Also, it is reasonable to expect that the details of the contact pressure distribution will depend on patient specific anatomical

information about the geometry of the bone, muscles and arteries in the limb at the location of application of the ERT. In practice, such patient specific details are not known. Consequently, it is desirable to supplement available experimental data with analysis of a simplified model which is not patient specific and which can provide an upper bound on the pressure applied by the ERT on the skin.

As mentioned earlier, here attention is focused on the prediction of the contact pressure between a nonlinear elastic ring and a rigid circular cylinder. The effects of the stockinette are also modeled and shown to significantly reduce the magnitudes of the maximum and average contact pressures. This model is expected to produce an upper bound on the contact pressure since flexibility of the limb will tend to decrease the deformations of the ERT and tend to increase the effective contact area between the ERT and the skin, both of which will tend to reduce the contact pressure.

The main objective of this paper is to examine interesting mechanical phenomena associated with the modeling of this problem. Specifically, here a hierarchy of theories of a Cosserat curve is developed which incorporate different levels of complexity and which helps identify the most significant mechanical phenomena needed to model the problem. In all cases the ring is modeled as an incompressible, isotropic elastic material.

As a first attempt to predict this contact pressure it is natural to consider a nonlinear version of the classical Lame problem where internal pressure is applied to a circular ring with a rectangular cross-section. Specifically, in its stress-free reference configuration the ring is assumed to have radial thickness H and axial width W. The simple analysis of the ring, which is based on the free body diagram shown in Fig. 1, usually is applied to linear analysis of a thin ring. In particular, it will be shown that for this contact problem it is essential to model the effects of cross-sectional deformation in the rod. This is consistent with results for a linear contact problem reported in Naghdi and Rubin (1989).

The simplest approach is described in Section 2 and is based on a simple nonlinear analysis of the problem sketched in Fig. 1. Section 3 summarizes an exact axisymmetric plane strain nonlinear elasticity solution. However, closed form exact solutions of the three-dimensional theory are limited to simple functional forms of the strain energy. Therefore, to include more general material nonlinearity the problem is modeled using the theory of a Cosserat curve (Section 4) which includes the effects of cross-sectional deformation and bending. Also, within the context of the Cosserat theory, the effect of bending can be eliminated to obtain a simpler model of a Cosserat generalized string which includes the cross-section deformation

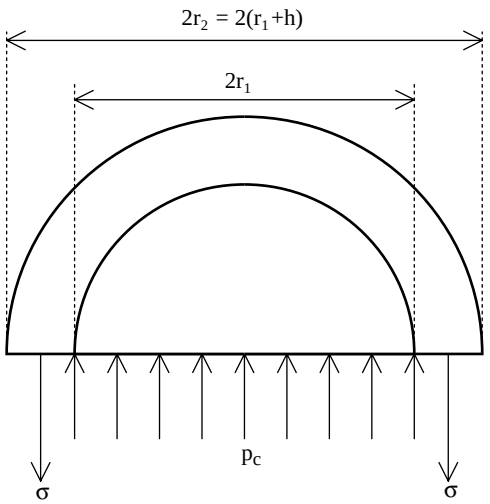

Fig. 1. Sketch of the deformed configuration of the simple model of the ring.

(Section 5) but no bending strength. Section 6 considers the case of uniaxial stress and the results in Section 7 indicate that the theory of a generalized Cosserat string is sufficiently accurate to model most aspects of the ERT device. Experimental results described in Section 8 indicate that a modified strain energy function is needed to model the uniaxial stress response of the ERT device. Section 9 uses a constrained form of the theory of a Cosserat generalized string to model the effects of the toroidal shape of the ERT ring. The results of the Cosserat theory are shown to be reasonably accurate relative to a finite element analysis described in Section 10. Section 11 describes modifications of the Cosserat and finite element models which include the influence of the stockinette. In particular, the Cosserat model is used to show that increasing the thickness of the stockinette can cause significant reduction in the maximum and average contact pressures applied by the ERT. Finally, conclusions are presented in Section 12.

2. Simple analysis

Here, the ERT is modeled as a circular ring with rectangular cross-section. In its stress-free reference configuration the ring has inner radius R_1, outer radius R_2, mean radius $\overline{R}$, radial thickness H and width W. Similarly, in its deformed configuration the ring has inner radius r_1, outer radius r_2, mean radius $\bar{r}$, radial thickness h and axial width w, so that

$$\overline{R} = \frac{R_1 + R_2}{2}, \qquad H = R_2 - R_1, \qquad \bar{r} = \frac{r_1 + r_2}{2}, \qquad h = r_2 - r_1. \tag{2.1}$$

The inner surface of the ring is subjected to the contact pressure p_c and its outer surface and edges are traction free (see Fig. 1). Moreover, the ring is assumed to be made of an incompressible, isotropic nonlinear elastic material.

The simple analysis of equilibrium in the vertical direction replaces the pressure applied by the tissue on the ring with a pressure at the base (like that associated with a liquid in equilibrium) and it assumes that the circumferential Cauchy stress σ (force per unit present area) is uniform through the thickness of the ring. Then, force equilibrium in the vertical direction yields the standard equation

$$p_c = \frac{h\sigma}{r_1}. \tag{2.2}$$

Next, introducing the stretches $\{a, b, \lambda\}$

$$a = \frac{w}{W}, \qquad b = \frac{h}{H} = \frac{r_2 - r_1}{R_2 - R_1}, \qquad \lambda = \frac{\bar{r}}{\overline{R}} = \frac{r_1 + r_2}{R_1 + R_2}, \tag{2.3a–c}$$

the incompressibility condition requires

$$ab\lambda = 1. \tag{2.4}$$

Then, the Cauchy stress σ can be related to the engineering stress Π (first Piola–Kirchhoff stress, i.e. the force per unit reference area) by the formula

$$hw\sigma = HW\Pi, \quad \sigma = \lambda\Pi, \tag{2.5}$$

and Eq. (2.2) can be rewritten in the form

$$p_c = \left[\frac{b\bar{r}}{r_1}\right]\frac{H\Pi}{\overline{R}}. \tag{2.6}$$

Furthermore, for the simple analysis it is assumed that the ring is so thin ($H/\overline{R} \ll 1$) that the pressure is negligible relative to the circumferential stress σ so the ring in a state of uniaxial stress. Within the context of this assumption the stretches a and b are equal

$$a = b = \frac{1}{\sqrt{\lambda}}, \tag{2.7}$$

and (2.6) becomes

$$p_c = \frac{H\Pi}{\overline{R}\sqrt{\lambda}\left\{1 - \frac{H}{2\overline{R}\lambda^{3/2}}\right\}}. \tag{2.8}$$

Once a form for Π as a function of λ is specified

$$\Pi = \Pi(\lambda), \tag{2.9}$$

Eq. (2.8) can be used to estimate the pressure applied by the ring. Also, the stretch λ_1 based on the inner radius r_1 is calculated by

$$\lambda_1 = \frac{r_1}{R_1}. \tag{2.10}$$

3. Axisymmetric plane strain analysis

Rivlin (1949) considered a number of problems of large deformation of nonlinear isotropic incompressible elastic materials which include a generalization of the Lame problem. For simplicity, the relevant results will be briefly developed in this section for a specific strain energy function. In particular, here a material point, which is located by the radius R in the reference configuration, is deformed to the radius r in the present configuration. Also, the equilibrium equations and boundary conditions are written in terms of the present radius, and the components of the Cauchy stress $\mathbf{T}^*$. Here, a superposed $(*)$ is used to distinguish quantities related to the three-dimensional theory from other quantities introduced later related to the Cosserat theory which use the same symbol but without the superposed $(*)$. Specifically, for the axisymmetric problem under consideration the cylindrical polar base vectors $\{\mathbf{e}_r, \mathbf{e}_\theta, \mathbf{e}_3\}$ are related to the fixed rectangular Cartesian base vectors $\mathbf{e}_i$ $(i = 1, 2, 3)$ by the standard formulas

$$\mathbf{e}_r = \cos\theta\,\mathbf{e}_1 + \sin\theta\,\mathbf{e}_2, \qquad \mathbf{e}_\theta = -\sin\theta\,\mathbf{e}_1 + \cos\theta\,\mathbf{e}_2, \tag{3.1}$$

and the Cauchy stress $\mathbf{T}^*$ is expressed in terms of its nonzero components

$$\mathbf{T}^* = T^*_{rr}\mathbf{e}_r \otimes \mathbf{e}_r + T^*_{\theta\theta}\mathbf{e}_\theta \otimes \mathbf{e}_\theta + T^*_{33}\mathbf{e}_3 \otimes \mathbf{e}_3, \tag{3.2}$$

where the symbol $\otimes$ denoted the tensor product. Moreover, in the absence of body force and inertia terms the only nontrivial equilibrium equation becomes

$$\frac{\partial T^*_{rr}}{\partial r} + \frac{T^*_{rr} - T^*_{\theta\theta}}{r} = 0. \tag{3.3}$$

Here, the position vectors $\mathbf{X}^*$ in the reference configuration and $\mathbf{x}^*$ in the present configuration are specified by

$$\begin{aligned} &\mathbf{X}^* = R\mathbf{e}_r + X_3\mathbf{e}_3, \qquad \mathbf{x}^* = \hat{r}(R)\mathbf{e}_r + x_3\mathbf{e}_3, \\ &r = \hat{r}(R), \quad x_3 = aX_3, \quad R_1 \leqslant R \leqslant R_2, \quad -\frac{W}{2} \leqslant X_3 \leqslant \frac{W}{2}, \end{aligned} \tag{3.4}$$

where the function $\hat{r}(R)$ and the constant stretch a need to be determined by the solution. It then follows from (3.4) that the deformation gradient $\mathbf{F}^*$ and the dilatation J^* become

$$\mathbf{F}^* = \frac{\mathrm{d}r}{\mathrm{d}R}(\mathbf{e}_r \otimes \mathbf{e}_r) + \frac{r}{R}(\mathbf{e}_\theta \otimes \mathbf{e}_\theta) + a(\mathbf{e}_3 \otimes \mathbf{e}_3), \qquad J^* = \det(\mathbf{F}^*) = a\frac{r}{R}\frac{\mathrm{d}r}{\mathrm{d}R}. \tag{3.5}$$

Thus, the nonlinear form of the incompressibility condition requires

$$a\frac{r}{R}\frac{\mathrm{d}r}{\mathrm{d}R}=1. \tag{3.6}$$

Furthermore, using the kinematic conditions that

$$r_1=\hat{r}(R_1),\qquad r_2=\hat{r}(R_2), \tag{3.7}$$

Eq. (3.6) can be integrated to obtain

$$r=\sqrt{r_1^2+\frac{1}{a}(R^2-R_1^2)},\qquad R=\sqrt{R_1^2+a(r^2-r_1^2)},\qquad r_2=\sqrt{r_1^2+\frac{R_2^2-R_1^2}{a}}. \tag{3.8a–c}$$

The boundary conditions on the inner and outer surfaces of the ring require

$$T^*_{rr}(r_1)=-p_{\mathrm{c}},\qquad T^*_{rr}(r_2)=0. \tag{3.9}$$

Also, the condition that the ends ($X_3=\pm W/2$) are stress free is approximated in a St Venant sense using the condition that the total axial force applied to these ends vanishes

$$2\pi\int_{r_1}^{r_2}T^*_{33}r\,\mathrm{d}r=0. \tag{3.10}$$

For the simple case of an incompressible isotropic Neo–Hookean nonlinear elastic material, the specific (per unit mass) strain energy function Σ^* is expressed in terms of the first invariant of the left Cauchy–Green deformation tensor $\mathbf{B}^*$, such that

$$\rho_0^*\Sigma^*=\frac{1}{6}f(\alpha^*),\qquad f(\alpha^*)=E(\alpha^*-3),\qquad \alpha^*=\mathbf{B}^*\cdot\mathbf{I},\qquad \mathbf{B}^*=\mathbf{F}^*\mathbf{F}^{*\mathrm{T}}, \tag{3.11a–d}$$

where ρ_0^* is the reference mass density and E is the zero-stress value of Young's modulus. Then, the constitutive equation for the stress becomes

$$\begin{aligned}&\mathbf{T}^*=-\gamma^*\mathbf{I}+\frac{1}{3}\frac{\mathrm{d}f}{\mathrm{d}\alpha^*}\mathbf{B}^*,\\&T^*_{rr}=-\gamma^*+\frac{E}{3}\left[\frac{R^2}{a^2r^2}\right],\quad T^*_{\theta\theta}=-\gamma^*+\frac{E}{3}\left[\frac{r^2}{R^2}\right],\quad T^*_{33}=-\gamma^*+\frac{Ea^2}{3},\end{aligned} \tag{3.12}$$

where γ^* is an arbitrary function due to the incompressibility constraint. Now, with the help of (3.8) the equilibrium equation (3.3) can be solved, subject to the boundary conditions (3.9) to obtain

$$\begin{aligned}&T^*_{rr}=-p_{\mathrm{c}}+\frac{E}{6a^2}\left[\frac{(r^2-r_1^2)(ar_1^2-R_1^2)}{r^2r_1^2}+a\ln\left\{\frac{[R_1^2+a(r^2-r_1^2)]r_1^2}{R_1^2r^2}\right\}\right],\\&T^*_{\theta\theta}=T^*_{rr}+\frac{E}{3}\left[\frac{r^2}{R^2}-\frac{R^2}{a^2r^2}\right],\qquad T^*_{33}=T^*_{rr}+\frac{E}{3}\left[a^2-\frac{R^2}{a^2r^2}\right].\end{aligned} \tag{3.13}$$

Next, using the boundary condition on T^*_{rr} at $r=r_2$, the contact pressure p_{c} is determined by the expression

$$p_{\mathrm{c}}=\frac{E}{6a^2}\left[\frac{(r_2^2-r_1^2)(ar_1^2-R_1^2)}{r_1^2r_2^2}+a\ln\left\{\frac{R_2^2r_1^2}{R_1^2r_2^2}\right\}\right]. \tag{3.14}$$

Furthermore, the boundary condition (3.10) can be written in the form

$$-\frac{(r_2^2-r_1^2)[(R_1^2-ar_1^2)+2ar_2^2(1-a^3)]}{R_1^2r_2^2}+\ln\left[\frac{R_2^2r_1^2}{R_1^2r_2^2}\right]=0. \tag{3.15}$$

Thus, the solution is obtained by specifying values for $\{E, R_1, R_2\}$ and r_1. Then, with the help of (3.8c), the condition (3.15) is solved iteratively for the stretch a. Once a is known, the contact pressure p_c is determined by (3.14) and the stretches $\{b, \lambda, \lambda_1, \lambda_2\}$ are determined by (2.3b,c) and (2.10).

4. Theory of a Cosserat curve

The theory of a Cosserat curve is a nonlinear continuum theory (e.g. Antman, 1972, 1995; Green et al., 1974a,b) that can be used to model the ring. Here, for convenience use is made of the notation employed in Rubin (2000). The static form of this theory models the ring as a space curve (or rod) whose material points in the deformed configuration are located by the position vector $\mathbf{x}$, which is a function of one convected coordinate θ^3. In addition, at each point of the rod, two director vectors $\mathbf{d}_\alpha$ ($\alpha = 1, 2$) are introduced to model deformations of line elements in the rod's cross-section. The kinematics of the stress-free reference configuration are specified by

$$\mathbf{X} = \mathbf{X}(\theta^3), \qquad \mathbf{D}_\alpha = \mathbf{D}_\alpha(\theta^3), \qquad \mathbf{D}_3 = \mathbf{X}_{,3}, \qquad \mathbf{D}_1 \times \mathbf{D}_2 \cdot \mathbf{D}_3 > 0, \qquad D_{33}^{1/2} = |\mathbf{D}_3|, \tag{4.1}$$

where a comma denotes partial differentiation with respect to θ^3. Also, the kinematics of the deformed present configuration are specified by

$$\mathbf{x} = \mathbf{x}(\theta^3), \qquad \mathbf{d}_\alpha = \mathbf{d}_\alpha(\theta^3), \qquad \mathbf{d}_3 = \mathbf{x}_{,3}, \qquad \mathbf{d}_1 \times \mathbf{d}_2 \cdot \mathbf{d}_3 > 0, \qquad d_{33}^{1/2} = |\mathbf{d}_3|. \tag{4.2}$$

The balance laws of the Cosserat theory can be developed by a direct approach or they can be motivated from the three-dimensional theory by using the kinematic assumptions that the three-dimensional position vectors $\mathbf{X}^*$ and $\mathbf{x}^*$ are expressed in the forms

$$\mathbf{X}^* = \mathbf{X} + \theta^\alpha \mathbf{D}_\alpha, \qquad \mathbf{x}^* = \mathbf{x} + \theta^\alpha \mathbf{d}_\alpha, \tag{4.3}$$

where for a rectangular cross-section

$$|\theta^1| \leqslant \pm\frac{W}{2}, \qquad |\theta^2| = \pm\frac{H}{2}. \tag{4.4}$$

Here, attention is confined to equilibrium so the balances of linear and director momentum become

$$m\mathbf{b} + \mathbf{t}^3_{,3} = 0, \qquad m\mathbf{b}^\alpha - \mathbf{t}^\alpha + \mathbf{m}^\alpha_{,3} = 0, \tag{4.5}$$

where the assigned fields $m\mathbf{b}$ and $m\mathbf{b}^\alpha$ are due to body force and tractions on the lateral surface of the rod, $\mathbf{t}^i$ are intrinsic director couples, and $\mathbf{t}^3$ is the force and $\mathbf{m}^\alpha$ are the couples applied to the rod's end. Also, by introducing the second order tensor $\mathbf{T}$

$$d_{33}^{1/2}\mathbf{T} = \mathbf{t}^i \otimes \mathbf{d}_i + \mathbf{m}^\alpha \otimes \mathbf{d}_{\alpha,3} \tag{4.6}$$

the balance of angular momentum requires $\mathbf{T}$ to be symmetric

$$\mathbf{T} = \mathbf{T}^{\mathrm{T}}. \tag{4.7}$$

In (4.6) and throughout the text, the usual summation convention is used for repeated indices with Latin indices having the range ($i = 1, 2, 3$) and Greek indices having the range ($\alpha = 1, 2$).

For an elastic rod it is convenient to introduce the deformation tensor $\mathbf{F}$ associated with homogeneous deformations (when $\mathbf{F}$ is independent of θ^3) and the vectors $\boldsymbol{\beta}_\alpha$ associated with inhomogeneous deformations by the formulas

$$\mathbf{F} = \mathbf{d}_i \otimes \mathbf{D}^i, \qquad \boldsymbol{\beta}_\alpha = \mathbf{F}^{-1}\mathbf{d}_{\alpha,3} - \mathbf{D}_{\alpha,3} \tag{4.8}$$

where the reciprocal vectors $\mathbf{D}^i$ and $\mathbf{d}^i$ are defined in terms of the Kronecker delta δ^j_i such that

$$\mathbf{D}_i \cdot \mathbf{D}^j = \delta^j_i, \qquad \mathbf{d}_i \cdot \mathbf{d}^j = \delta^j_i. \tag{4.9}$$

Furthermore, for a constrained elastic rod the kinetic quantities $\{\mathbf{T}, \mathbf{t}^i, \mathbf{m}^\alpha\}$ separate additively into parts $\{\widehat{\mathbf{T}}, \hat{\mathbf{t}}^i, \hat{\mathbf{m}}^\alpha\}$ derived from the strain energy function Σ and parts $\{\overline{\mathbf{T}}, \bar{\mathbf{t}}^i, \bar{\mathbf{m}}^\alpha\}$ characterizing the constraint responses

$$\begin{aligned} &\mathbf{T} = \widehat{\mathbf{T}} + \overline{\mathbf{T}}, \qquad \mathbf{t}^i = \hat{\mathbf{t}}^i + \bar{\mathbf{t}}^i, \qquad \mathbf{m}^\alpha = \hat{\mathbf{m}}^\alpha + \bar{\mathbf{m}}^\alpha, \qquad \Sigma = \Sigma(\mathbf{C}, \boldsymbol{\beta}_\alpha), \\ &\mathbf{C} = \mathbf{F}^{\mathrm{T}}\mathbf{F}, \qquad d_{33}^{1/2}\widehat{\mathbf{T}} = 2m\mathbf{F}\frac{\partial \Sigma}{\partial \mathbf{C}}\mathbf{F}^{\mathrm{T}}, \qquad \hat{\mathbf{m}}^\alpha = m\mathbf{F}^{-\mathrm{T}}\frac{\partial \Sigma}{\partial \boldsymbol{\beta}_\alpha}, \end{aligned} \tag{4.10}$$

where m is related to the mass per unit length of the rod. Moreover, the work in Rubin (1996, 2000) derived restrictions on the strain energy function which ensure that the Cosserat theory will predict exact solutions for all homogeneous deformations of a rod made from a uniform, homogeneous, elastic material. In particular, for the circular rod under consideration here, the strain energy function can be written in the form

$$m\Sigma = m\Sigma^*(\mathbf{C}) + \frac{1}{2}D_{33}^{-1/2}HW\mathbf{K}^{\alpha\beta} \cdot (\boldsymbol{\beta}_\alpha \otimes \boldsymbol{\beta}_\beta), \quad m = \rho_0^* D_{33}^{1/2}HW, \tag{4.11}$$

where the three-dimensional strain energy Σ^* can be a general function of its argument and where it has been assumed that the strain energy is a quadratic function of the inhomogeneous strains $\boldsymbol{\beta}_\alpha$, with $\mathbf{K}^{\alpha\beta}$ being constant tensors.

For later convenience, in addition to the incompressibility constraint which requires the dilatation J to remain constant, shear deformation in the rod's cross-section is constrained so that the constraints become

$$J = \det(\mathbf{F}) = 1, \qquad \mathbf{d}_1 \cdot \mathbf{d}_2 = 0. \tag{4.12}$$

It then follows from the work in Rubin (2000, Sec. 5.9) that the constraint responses are given by

$$\begin{aligned} &d_{33}^{1/2}\overline{\mathbf{T}} = -HW[\gamma\mathbf{I} + \gamma^{12}(\mathbf{d}_1 \otimes \mathbf{d}_2 + \mathbf{d}_2 \otimes \mathbf{d}_1)], \qquad \bar{\mathbf{t}}^1 = -HW[\gamma\mathbf{d}^1 + \gamma^{12}\mathbf{d}_2], \\ &\bar{\mathbf{t}}^2 = -HW[\gamma\mathbf{d}^2 + \gamma^{12}\mathbf{d}_1], \qquad \bar{\mathbf{t}}^2 = -HW[\gamma\mathbf{d}^3], \qquad \bar{\mathbf{m}}^\alpha = 0, \end{aligned} \tag{4.13}$$

where γ and γ^{12} are arbitrary functions of θ^3. Next, confining attention to the case of an isotropic material, the three-dimensional strain energy function Σ^* is taken to be a general function of the invariant α

$$\rho_0^*\Sigma^* = \frac{1}{6}f(\alpha), \qquad \alpha = \mathbf{C} \cdot \mathbf{I} = \mathbf{B} \cdot \mathbf{I}, \qquad \mathbf{B} = \mathbf{F}\mathbf{F}^{\mathrm{T}}, \qquad f(3) = 0, \qquad \frac{\mathrm{d}f}{\mathrm{d}\alpha}(3) = E, \tag{4.14}$$

where E is the zero tension Young's modulus and the tensors $\mathbf{K}^{\alpha\beta}$ are specified so that (Rubin, 2000, Sec. 5.26)

$$\mathbf{K}^{12} = \mathbf{K}^{21} = 0. \tag{4.15}$$

Consequently, the constitutive equations become

$$\begin{aligned} &d_{33}^{1/2}\mathbf{T} = HW\left[-\gamma\mathbf{I} - \gamma^{12}(\mathbf{d}_1 \otimes \mathbf{d}_2 + \mathbf{d}_2 \otimes \mathbf{d}_1) + \frac{1}{3}\frac{\mathrm{d}f}{\mathrm{d}\alpha}\mathbf{B}\right], \\ &\mathbf{t}^i = [d_{33}^{1/2}\mathbf{T} - \mathbf{m}^\alpha \otimes \mathbf{d}_{\alpha,3}] \cdot \mathbf{d}^i, \\ &\mathbf{m}^1 = D_{33}^{-1/2}HW\mathbf{F}^{-\mathrm{T}}\mathbf{K}^{11}\boldsymbol{\beta}_1, \qquad \mathbf{m}^2 = D_{33}^{-1/2}HW\mathbf{F}^{-\mathrm{T}}\mathbf{K}^{22}\boldsymbol{\beta}_2. \end{aligned} \tag{4.16}$$

Now, the kinematics of the ring in its reference configuration are given by

$$\begin{aligned} &\mathbf{X} = \overline{R}\mathbf{e}_r(\theta), \qquad \mathbf{D}_1 = \mathbf{e}_3, \qquad \mathbf{D}_2 = \mathbf{e}_r(\theta), \qquad \theta = \frac{\theta^3}{\overline{R}}, \quad 0 \leqslant \theta^3 \leqslant 2\pi\overline{R}, \\ &\mathbf{D}_3 = \mathbf{X}_{,3} = \mathbf{e}_\theta, \qquad D^{1/2} = \mathbf{D}_1 \times \mathbf{D}_2 \cdot \mathbf{D}_3 = 1, \qquad \mathbf{D}^i = \mathbf{D}_i, \qquad D_{33}^{1/2} = |\mathbf{D}_3| = 1, \end{aligned} \tag{4.17}$$

where the mean radius $\overline{R}$ is defined in (2.1) and $\mathbf{D}_3$ is a tangent vector to the reference curve. Also, the kinematics of the present deformed configuration are given by

$$\begin{aligned}
&\mathbf{x} = \bar{r}\mathbf{e}_r(\theta), \qquad \mathbf{d}_1 = a\mathbf{e}_3, \qquad \mathbf{d}_2 = b\mathbf{e}_r(\theta), \qquad \mathbf{d}_3 = \mathbf{x}_{,3} = \lambda\mathbf{e}_\theta,\\
&d_{33}^{1/2} = |\mathbf{d}_3| = \lambda, \qquad \mathbf{d}^1 = \frac{1}{a}\mathbf{e}_3, \qquad \mathbf{d}^2 = \frac{1}{b}\mathbf{e}_r, \qquad \mathbf{d}^3 = \frac{1}{\lambda}\mathbf{e}_\theta,\\
&\mathbf{F} = \mathbf{d}_i \otimes \mathbf{D}^i = a\mathbf{e}_3 \otimes \mathbf{e}_3 + b\mathbf{e}_r \otimes \mathbf{e}_r + \lambda\mathbf{e}_\theta \otimes \mathbf{e}_\theta, \qquad J = \det \mathbf{F} = ab\lambda,\\
&\boldsymbol{\beta}_1 = \mathbf{F}^{-1}\mathbf{d}_{1,3} - \mathbf{D}_{1,3} = 0, \qquad \boldsymbol{\beta}_2 = \mathbf{F}^{-1}\mathbf{d}_{2,3} - \mathbf{D}_{2,3} = \frac{1}{\overline{R}}\left[\frac{b}{\lambda} - 1\right]\mathbf{e}_\theta,
\end{aligned} \tag{4.18}$$

where the stretches $\{a, b, \lambda\}$ are defined by (2.3c). Thus, using the expression for $\mathbf{K}^{22}$ in Rubin (2000, Sec. 5.26) (with $\mu^* = E/3$ and $\nu^* = 1/2$, and H interchanged with W, and $\mathbf{M}_i = \mathbf{D}_i$) the constitutive equations (4.16) yield

$$\begin{aligned}
&\mathbf{t}^1 = \frac{HW}{a}\left[-\gamma + \frac{1}{3}\frac{\mathrm{d}f}{\mathrm{d}\alpha}a^2\right]\mathbf{e}_3 - HWb[\gamma^{12}]\mathbf{e}_r,\\
&\mathbf{t}^2 = \frac{HW}{b}\left[-\gamma + \frac{1}{3}\frac{\mathrm{d}f}{\mathrm{d}\alpha}b^2\right]\mathbf{e}^r - HWa[\gamma^{12}]\mathbf{e}_3,\\
&\mathbf{t}^3 = HW\Pi\mathbf{e}_\theta, \qquad \Pi = \left[\frac{1}{\lambda}\left(-\gamma + \frac{1}{3}\frac{\mathrm{d}f}{\mathrm{d}\alpha}\lambda^2\right) - \frac{EIb}{HW\lambda^2\overline{R}^2}\left(\frac{b}{\lambda} - 1\right)\right],\\
&\mathbf{m}^1 = 0, \qquad \mathbf{m}^2 = \frac{EI}{\lambda\overline{R}}\left(\frac{b}{\lambda} - 1\right)\mathbf{e}_\theta, \qquad I = \frac{H^3W}{12},
\end{aligned} \tag{4.19}$$

where I is the second moment of the area of the cross-section relative to the θ^2 coordinate and Π is the average engineering circumferential stress.

Next, it is convenient to formulate the more general problem shown in Fig. 2 where the deformed ring is subjected to internal pressure p_1, external pressure p_2, shear forces $\{V_1, V_2\}$ and moments $\{M_1, M_2\}$ on the ring's axial surfaces acting in the circumferential directions. Specifically, the traction vectors applied to the lateral boundary of the rod are specified by

$$\begin{aligned}
&\mathbf{t}^*\left(\frac{W}{2}, \theta^2, \theta^3\right) = \tau_2(\theta^2)\mathbf{e}_r + \sigma_2(\theta^2)\mathbf{e}_3, \qquad \mathbf{t}^*\left(-\frac{W}{2}, \theta^2, \theta^3\right) = -\tau_1(\theta^2)\mathbf{e}_r - \sigma_1(\theta^2)\mathbf{e}_3,\\
&\mathbf{t}^*\left(\theta^1, \frac{H}{2}, \theta^3\right) = -p_2\mathbf{e}_r, \qquad \mathbf{t}^*\left(\theta^1, -\frac{H}{2}, \theta^3\right) = p_1\mathbf{e}_r,
\end{aligned} \tag{4.20}$$

where the pressures $\{p_1, p_2\}$ are independent of θ^i and the stresses $\{\sigma_1, \sigma_2, \tau_1, \tau_2\}$ depend on θ^2, such that

$$\begin{aligned}
&\int_{-H/2}^{H/2}[\bar{r} + \theta^2 b]\tau_1(\theta^2)\,\mathrm{d}\theta^2 = \frac{V_1}{2\pi b}, \qquad \int_{-H/2}^{H/2}[\bar{r} + \theta^2 b]\tau_1(\theta^2)\theta^2\,\mathrm{d}\theta^2 = 0,\\
&\int_{-H/2}^{H/2}[\bar{r} + \theta^2 b]\tau_2(\theta^2)\,\mathrm{d}\theta^2 = \frac{V_2}{2\pi b}, \qquad \int_{-H/2}^{H/2}[\bar{r} + \theta^2 b]\tau_2(\theta^2)\theta^2\,\mathrm{d}\theta^2 = 0,\\
&\int_{-H/2}^{H/2}[\bar{r} + \theta^2 b]\sigma_1(\theta^2)\,\mathrm{d}\theta^2 = 0, \qquad \int_{-H/2}^{H/2}[\bar{r} + \theta^2 b]\sigma_1(\theta^2)\theta^2\,\mathrm{d}\theta^2 = -\frac{M_1}{2\pi b^2},\\
&\int_{-H/2}^{H/2}[\bar{r} + \theta^2 b]\sigma_2(\theta^2)\,\mathrm{d}\theta^2 = 0, \qquad \int_{-H/2}^{H/2}[\bar{r} + \theta^2 b]\sigma_2(\theta^2)\theta^2\,\mathrm{d}\theta^2 = -\frac{M_2}{2\pi b^2}.
\end{aligned} \tag{4.21}$$

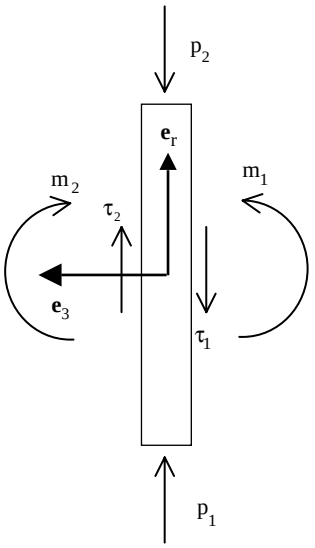

Fig. 2. Sketch of the generalized loading on a ring element.

In these expressions, the shear forces $\{V_1, V_2\}$ and the moments $\{M_1, M_2\}$ are measured per unit length $d\theta^3$. It then follows from the expressions in Rubin (2000, Sec. 5.26) (with H and W interchanged) that in the absence of body force the assigned fields are given by

$$m\mathbf{b} = \left[\frac{(V_1+V_2)}{2\pi\overline{R}} + \frac{w}{\overline{R}}(r_1p_1 - r_2p_2)\right]\mathbf{e}_r, \qquad m\mathbf{b}^1 = \frac{W(-V_1+V_2)}{4\pi\overline{R}}\mathbf{e}_r,$$
$$m\mathbf{b}^2 = -\left[\frac{Hw}{2\overline{R}}(r_1p_1 + r_2p_2)\right]\mathbf{e}_r + \left[\frac{(M_1+M_2)}{2\pi\overline{R}b}\mathbf{e}_3\right]. \tag{4.22}$$

Furthermore, it can be shown (Rubin, 2000, Sec. 5.26) that the moment (per unit length $d\theta^3$) applied by the stresses (4.20) on the lateral surfaces of the rod about its centerline is given by

$$\mathbf{d}_\alpha \times m\mathbf{b}^\alpha = \left[\frac{w}{2}\left\{\frac{-V_1+V_2}{2\pi\overline{R}}\right\} + \frac{(M_1+M_2)}{2\pi\overline{R}}\right]\mathbf{e}_\theta, \tag{4.23}$$

which includes both the effects of the shear forces and the pure moments.

Next, with the help of the incompressibility condition (4.12), and the expressions (4.18), (4.19) and (4.22), the equilibrium equations (4.5) reduce to

$$\frac{(V_1+V_2)}{2\pi} + w(r_1p_1 - r_2p_2) - HW\Pi = 0, \tag{4.24a}$$

$$\frac{Hw}{2\overline{R}}[r_1p_1 + r_2p_2] + \frac{HW}{3}\frac{\mathrm{d}f}{\mathrm{d}\alpha}\left(b - \frac{1}{\lambda^2b^3}\right) + \frac{EI}{\lambda\overline{R}^2}\left[\frac{b}{\lambda} - 1\right] = 0, \tag{4.24b}$$

$$M_1 + M_2 = \frac{w}{2}(V_1 - V_2), \tag{4.24c}$$

$$\gamma = \frac{1}{3}\frac{\mathrm{d}f}{\mathrm{d}\alpha}\frac{1}{\lambda^2b^2}, \qquad \gamma^{12} = \frac{(M_1+M_2)}{2\pi\overline{R}HWab}, \tag{4.24d,e}$$

where from (4.19) Π is given by

$$\Pi = \frac{1}{3}\frac{\mathrm{d}f}{\mathrm{d}\alpha}\left(\lambda - \frac{1}{\lambda^3 b^2}\right) - \frac{EIb}{HW\lambda^2\overline{R}^2}\left(\frac{b}{\lambda} - 1\right). \tag{4.25}$$

For most of the problems considered in the next sections the shear forces and moments vanish so that

$$V_1 = V_2 = M_1 = M_2 = \gamma^{12} = 0. \tag{4.26}$$

Then, (4.24b) can be solved for γ and the incompressibility condition (4.12) and (4.19) can be used to solve (4.24a) and (4.24c) for p_1 and p_2 to obtain

$$p_1 = \frac{b\overline{r}}{3r_1}\left[\frac{\mathrm{d}f}{\mathrm{d}\alpha}\left(\frac{1}{b^3\lambda^2} - b\right) + \frac{H}{2\overline{R}}\frac{\mathrm{d}f}{\mathrm{d}\alpha}\left(\lambda - \frac{1}{\lambda^3 b^2}\right) + \frac{3EI}{\lambda HW\overline{R}^2}\left(1 - \frac{b}{\lambda}\right)\left(1 + \frac{bH}{2\lambda\overline{R}}\right)\right], \tag{4.27a}$$

$$p_2 = \frac{b\overline{r}}{3r_2}\left[\frac{\mathrm{d}f}{\mathrm{d}\alpha}\left(\frac{1}{b^3\lambda^2} - b\right) - \frac{H}{2\overline{R}}\frac{\mathrm{d}f}{\mathrm{d}\alpha}\left(\lambda - \frac{1}{\lambda^3 b^2}\right) + \frac{3EI}{\lambda HW\overline{R}^2}\left(1 - \frac{b}{\lambda}\right)\left(1 - \frac{bH}{2\lambda\overline{R}}\right)\right]. \tag{4.27b}$$

Thus, for the problem under consideration in Section 3

$$p_1 = p_c, \qquad p_2 = 0, \tag{4.28}$$

and the relevant equations become

$$p_c = \left[\frac{b\overline{r}}{r_1}\right]\frac{H\Pi}{\overline{R}}, \qquad \Pi = \frac{1}{3}\frac{\mathrm{d}f}{\mathrm{d}\alpha}\left(\lambda - \frac{1}{\lambda^3 b^2}\right) + \frac{EIb}{HW\lambda^2\overline{R}^2}\left(1 - \frac{b}{\lambda}\right), \tag{4.29a,b}$$

$$\frac{\mathrm{d}f}{\mathrm{d}\alpha}\left(\frac{1}{b^3\lambda^2} - b\right) - \frac{H}{2\overline{R}}\frac{\mathrm{d}f}{\mathrm{d}\alpha}\left(\lambda - \frac{1}{\lambda^3 b^2}\right) + \frac{3EI}{\lambda HW\overline{R}^2}\left(1 - \frac{b}{\lambda}\right)\left(1 - \frac{bH}{2\lambda\overline{R}}\right) = 0, \tag{4.29c}$$

$$a = \frac{1}{b\lambda}, \qquad \alpha = a^2 + b^2 + \lambda^2, \tag{4.29d,e}$$

where (4.29a) is seen to be the same as (2.6).

5. Theory of a Cosserat generalized string

The theory of a Cosserat generalized string (Rubin, 2000, Sec. 5.30) is a special case of the Cosserat theory of rods where the effects of bending are ignored. This theory differs from simple string theory in that it models deformations of the string's cross-section and it can reproduce exact solutions for all homogeneous deformations of a uniform, homogeneous elastic material. The kinematics of the generalized string are the same as those of the rod (4.2) and (4.3), and the balance laws are the same as (4.5)–(4.7), except that the director couples $\mathbf{m}^\alpha$ are omitted

$$m\mathbf{b} + \mathbf{t}^3_{,3} = 0, \qquad m\mathbf{b}^\alpha - \mathbf{t}^\alpha = 0, \qquad d_{33}^{1/2}\mathbf{T} = \mathbf{t}^i \otimes \mathbf{d}_i \tag{5.1}$$

Also, the effects of bending are omitted so the strain energy takes the form

$$m\Sigma = m\Sigma^*(\mathbf{C}), \qquad \rho_0^*\Sigma^* = \frac{1}{6}f(\alpha), \tag{5.2}$$

instead of (4.11) with (4.14). Thus, the constitutive equations for the string subjected to the constraints (4.12) become

$$d_{33}^{1/2}\mathbf{T} = HW\left[-\gamma\mathbf{I} - \gamma^{12}(\mathbf{d}_1\otimes\mathbf{d}_2 + \mathbf{d}_2\otimes\mathbf{d}_1) + \frac{1}{3}\frac{\mathrm{d}f}{\mathrm{d}\alpha}\mathbf{B}\right], \qquad \mathbf{t}^i = d_{33}^{1/2}\mathbf{T}\cdot\mathbf{d}^i \tag{5.3}$$

instead of (4.16).

Now, using the relevant kinematics from (4.17) and (4.18), the equilibrium equations for the constrained string (4.24) and the constitutive equation (4.25) for Π reduce to

$$\frac{(V_1+V_2)}{2\pi} + w(r_1p_1 - r_2p_2) - HW\Pi = 0, \tag{5.4a}$$

$$\frac{w}{2\bar{R}}[r_1p_1 + r_2p_2] + \frac{W}{3}\frac{\mathrm{d}f}{\mathrm{d}\alpha}\left(b - \frac{1}{\lambda^2b^3}\right) = 0, \tag{5.4b}$$

$$M_1 + M_2 = \frac{w}{2}(V_1 - V_2), \tag{5.4c}$$

$$\gamma = \frac{1}{3}\frac{\mathrm{d}f}{\mathrm{d}\alpha}\frac{1}{\lambda^2b^2}, \qquad \gamma^{12} = \frac{(M_1+M_2)}{2\pi\bar{R}HWab}, \qquad \Pi = \frac{1}{3}\frac{\mathrm{d}f}{\mathrm{d}\alpha}\left(\lambda - \frac{1}{\lambda^3b^2}\right), \tag{5.4d–f}$$

where the bending term I has been set equal to zero. Moreover, for the case of a string associated with the conditions (4.26), Eqs. (4.29) reduce to

$$p_c = \left[\frac{b\bar{r}}{r_1}\right]\frac{H\Pi}{\bar{R}}, \qquad \Pi = \frac{1}{3}\frac{\mathrm{d}f}{\mathrm{d}\alpha}\left(\lambda - \frac{1}{\lambda^3b^2}\right), \tag{5.5a,b}$$

$$\left(\frac{1}{b^3\lambda^2} - b\right) - \frac{H}{2\bar{R}}\left(\lambda - \frac{1}{\lambda^3b^2}\right) = 0, \qquad a = \frac{1}{b\lambda}, \qquad \alpha = a^2 + b^2 + \lambda^2. \tag{5.5c–e}$$

6. Uniaxial stress

In order to compare the predictions of the more general theories with the simple analysis of Section 2 it is necessary to determine the constitutive equation for the engineering stress Π associated with uniaxial stress. As mentioned previously, both Cosserat theories of rods and generalized strings produce the exact three-dimensional solutions for homogeneous deformations. In particular, for uniaxial stress in the $\mathbf{d}_3$ direction with the axial stretch λ, the force $\mathbf{t}^3$ is related to the engineering stress Π by the equations

$$\mathbf{t}^3 = HW\Pi\frac{\mathbf{d}_3}{|\mathbf{d}_3|}, \qquad |\mathbf{d}_3| = \lambda. \tag{6.1}$$

Moreover, the three-dimensional strain energy is specified in the form (3.11a). Now, for uniaixal stress in the $\mathbf{e}_3$ direction, the deformation is specified by

$$\mathbf{x}^* = \frac{\theta^1}{\sqrt{\lambda}}\mathbf{e}_1 + \frac{\theta^2}{\sqrt{\lambda}}\mathbf{e}_2 + \lambda\mathbf{e}_3, \tag{6.2}$$

and the three-dimensional Cauchy stress becomes

$$\begin{aligned}&\mathbf{T}^* = T_{11}^*(\mathbf{e}_1\otimes\mathbf{e}_1) + T_{22}^*(\mathbf{e}_2\otimes\mathbf{e}_2) + T_{33}^*(\mathbf{e}_3\otimes\mathbf{e}_3) = -\gamma^*\mathbf{I} + \frac{1}{3}\frac{\mathrm{d}f}{\mathrm{d}\alpha^*}\mathbf{B}^*,\\ &T_{11}^* = T_{22}^* = -\gamma^* + \frac{1}{3\lambda}\frac{\mathrm{d}f}{\mathrm{d}\alpha^*} = 0, \qquad T_{33}^* = -\gamma^* + \frac{\lambda^2}{3}\frac{\mathrm{d}f}{\mathrm{d}\alpha^*}.\end{aligned} \tag{6.3}$$

Thus, the values of σ and Π in (2.5) to be used in the simple solution (2.6) become

$$\sigma = T^*_{33} = \frac{1}{3}\frac{df}{d\alpha^*}\left[\lambda^2 - \frac{1}{\lambda}\right], \qquad \Pi = \frac{1}{3}\frac{df}{d\alpha^*}\left[\lambda - \frac{1}{\lambda^2}\right], \qquad \alpha^* = \lambda^2 + \frac{2}{\lambda}. \tag{6.4a–c}$$

7. Comparison of the theories

When the function $f(\alpha^*)$ is specified in the form (3.11b) it is possible to compare the predictions of the simple solution of Section 2, and the Cosserat solutions of Sections 4 and 5 with the exact three-dimensional solution of Section 3. Specifically, the kinematics are defined by (2.3) and (2.10). The simple solution is characterized by (2.7), (2.8), (3.11b), (6.4b); the solution of a Cosserat rod is characterized by (3.11b), (4.29); the solution of a Cosserat generalized string is characterized by (3.11b), (5.5); and the exact solution is characterized by (3.8), (3.11b), (3.14), (3.15).

In practice, the ERT device has to occlude the blood vessels at a particular location on the limb of a specific patient who has a specific blood pressure. In choosing the appropriate ERT it is most convenient to measure the circumference of the limb at the location of application of the tourniquet and to calculate the desired stretch to correspond to the specific blood pressure. Consequently, it is most convenient to determine the applied pressure as a function of the stretch λ_1 of the inner radius (2.10) of the ERT.

Figs. 3 and 4 compare the predictions of: the exact 3D theory, a Cosserat rod, a Cosserat generalized string, and the simple analysis for a thick ring ($\overline{R}/H = 2$) and a thinner ring ($\overline{R}/H = 10$), respectively. Specifically, the normalized pressure ($p_c\overline{R}/H/E$), the relative pressure (p_c/Π) and the stretches a and b are plotted as functions of the inner stretch λ_1. The relative pressure (p_c/Π) is not presented for the exact solution since Π is only an average value of stress.

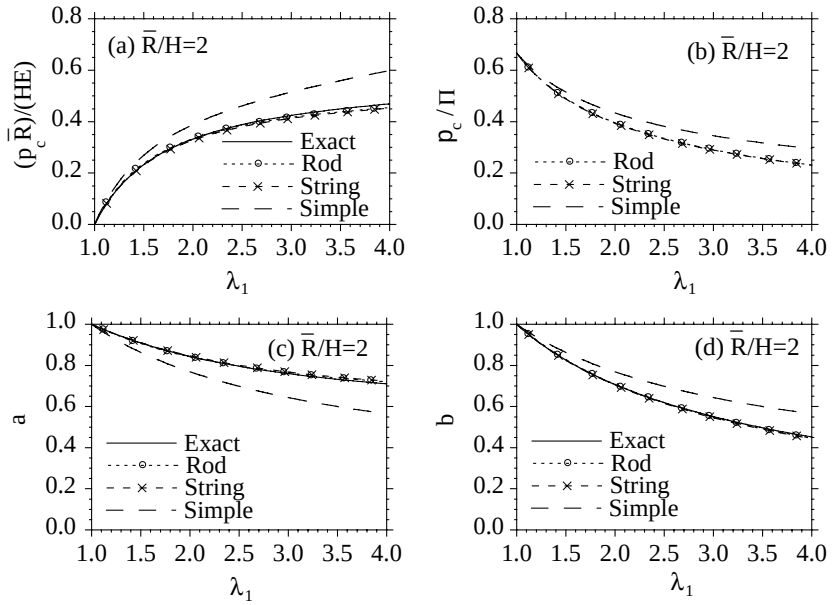

Fig. 3. Thick ring ($\overline{R}/H = 2$). Comparison of the predictions of: the exact 3D theory, a Cosserat rod, a Cosserat generalized string, and the simple analysis.

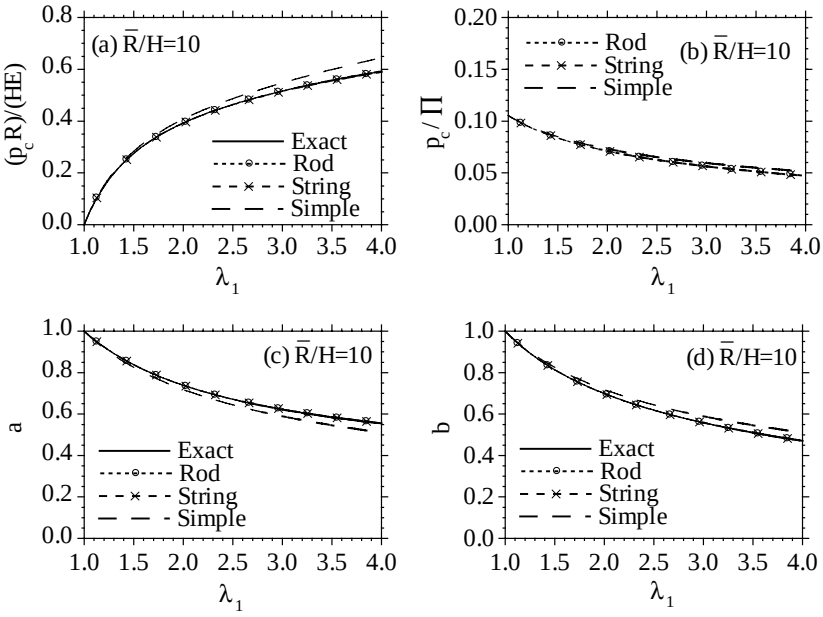

Fig. 4. Thinner ring ($\overline{R}/H = 10$). Comparison of the predictions of: the exact 3D theory, a Cosserat rod, a Cosserat generalized string, and the simple analysis.

The results in Figs. 3 and 4 indicate that for this problem the effects of bending stiffness are negligible since the results of a Cosserat generalized string nearly coincide with the exact solution and that of a Cosserat rod. In both cases the relative pressure (p_c/Π) decreases with increasing stretch λ_1. Moreover, the fact that the pressure p_c is not negligible relative to the average circumferential stress Π for the thick ring causes the stretches a and b to differ significantly from those predicted by the simple analysis which assumes uniaxial stress. This in turn causes the contact pressure p_c and the relative pressure (p_c/Π) to be incorrectly predicted by the simple analysis. However, as the ring becomes thinner this error decreases. Specifically, from Fig. 4 it can be seen that when $\overline{R}/H = 10$ this error is relatively small. Also, it is noted from Fig. 3 that the more exact solutions predict a larger value for the axial stretch a and a smaller value for the radial stretch b, relative to the simple solution. This is consistent with the fact that pressure p_c causes more radial contraction and less axial contraction than would be present in a state of uniaxial circumferential stress.

In summary, the main result of this section is that for thick rings the contact pressure p_c is not negligible relative to the average circumferential stress Π so it is necessary to use a more general theory which models the non-uniaxial stress state in the ring. Moreover, it has been shown that the Cosserat theory of a generalized string predicts accurate results for this problem even for relatively thick rings. Therefore, in the following analysis use will be made of the simpler theory of a Cosserat generalized string.

8. Experiments

One of the ERT devices developed by OHK Medical Devices Inc. is a torus, which in its unstressed reference configuration, has inner diameter D_1 and outer diameter D_2 given by

$$D_1 = 52\ \text{mm}, \qquad D_2 = 76\ \text{mm}, \tag{8.1}$$

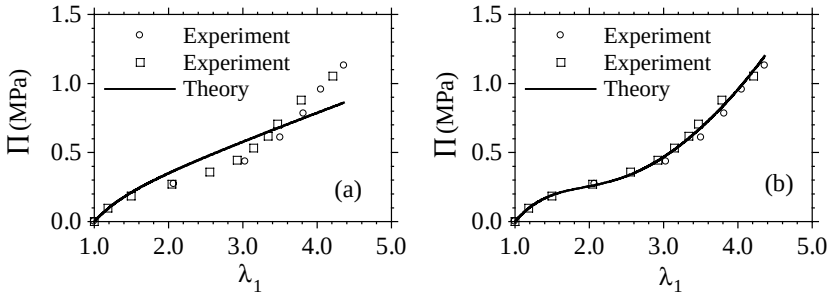

Fig. 5. Uniaxial stress. Comparison of theory and experiment using: (a) the simple strain energy function (3.11b) and (b) the modified strain energy (8.3).

so that the diameter of the circular cross-section is given by $(D_2 - D_1)/2$. The ring is made from a composition of silicone which was designed to have an elastic response that is compatible with the proposed application.

To determine the tensile properties of the ERT the ring was cut and the ends were pulled apart by coaxial forces. The engineering stress Π (force per unit reference cross-sectional area) and the stretch λ where measured to obtain the experimental values shown in Fig. 5a and b. Due to the toroidal shape of the ring in its unstressed configuration the stress in the cut stretched ring was not exactly uniaxial. However, this effect is negligible because the value of Π required to straighten the ring was only about 2.6 KPa. Fig. 5a shows results of two experiments on two different samples of the ring. Also, Fig. 5a shows an attempt to match the experimental data using (6.4b) with the simple constitutive assumption $f(\alpha^*)$ given in (3.11b)

$$\Pi = \frac{E}{3}\left[\lambda - \frac{1}{\lambda^2}\right], \quad E = 0.60 \text{ MPa}. \tag{8.2}$$

Obviously, this simple strain energy function cannot adequately model the experimental data. An improved strain energy function can be specified by taking $f(\alpha^*)$ in (3.11b) in form

$$f(\alpha^*) = \frac{3E_1}{m}\left[1 - \exp\left\{m\left(\frac{\alpha^*}{3} - 1\right)\right\}\right] + \frac{3E_2}{(1+n)}\left[\left\{\frac{\alpha^*}{3}\right\}^{n+1} - 1\right], \qquad E = E_1 + E_2, \tag{8.3}$$

where the constants E_1 and E_2 have the units of stress, the constants m and n are unitless and E is the zero stress Young's modulus. It then follows from (6.4) that for uniaxial stress

$$\Pi = \frac{1}{3}\left[E_1 \exp\left\{-m\left(\frac{\alpha^*}{3} - 1\right)\right\} + E_2\left\{\frac{\alpha^*}{3}\right\}^n\right]\left[\lambda - \frac{1}{\lambda^2}\right], \qquad \alpha^* = \lambda^2 + \frac{2}{\lambda}. \tag{8.4}$$

Furthermore, using this functional form together with the constants

$$E_1 = 0.45 \text{ MPa}, \quad m = 1.5, \qquad E_2 = 0.18 \text{ MPa}, \quad n = 0.82, \tag{8.5}$$

it is possible to match the experimental data quite accurately as shown in Fig. 5b.

9. An approximate analysis of the torus

Modeling the actual problem of the ERT device would require a two-dimensional axisymmetric nonlinear finite element calculation of the deformation of the toroidal ring which is in contact with soft tissue. The first simplifying approximation is to replace the soft tissue by a rigid cylinder. Cylinders of different radii

are used to expand the ring to different degrees of stretch. As the radius of the cylinder increases the contact area between the cylinder and the ring increases and the ring stretches circumferentially. From simple analysis similar to that in Section 2 it is clear that the radial force per unit circumferential length of the ring is controlled by the tensile force in the ring, which is mainly determined by the circumferential stretch and not the actual contact area. In contrast, the maximum and average contact pressures applied by the ring on the cylinder are sensitive to this contact area. Moreover, to model the development of this contact area it is necessary to model the changes in the initial circular cross-section of the ring.

To this end, an approximate model is proposed which models the torus as N adjacent disks (see Fig. 6 for $N = 8$). In its reference configuration, the Ith disk has internal radius ${}_IR_1$, external radius ${}_IR_2$, radial height ${}_IH$, axial width $\overline{W}$ and mean radius $\overline{R}$. In its deformed present configuration it has internal radius ${}_ir_1$, external radius ${}_ir_2$, radial height ${}_ih$ and axial width ${}_iw$. In this model shear forces and moments are applied between the disks to maintain the same mean radius $\bar{r}$ for all disks and to keep them from rotating. But, the disks are allowed to slide on each other in the sense that radial thickness of each disk can change independently. Also, the disks are modeled using the theory of a Cosserat generalized string discussed in Section 5 with the strain energy function (4.14) and (8.3).

More specifically, the reference torus is divided into N disks with equal widths $\overline{W}$ and the reference axial locations $\{{}_IZ^*, {}_{I+1}Z^*\}$ of the edges of the Ith disk are given by

$$\overline{W} = \frac{D_2 - D_1}{2N}, \qquad {}_IZ^* = -\left[\frac{D_2 - D_1}{4}\right] + (I-1)\overline{W} \quad \text{for } I = 1, 2, \ldots, N+1. \tag{9.1}$$

Then, the heights ${}_IH$ are specified so that the Ith disk has the same cross-sectional area as the corresponding portion of the torus

$$\begin{aligned} {}_IH &= \frac{1}{\overline{W}}\left[\frac{D_2 - D_1}{4}\right]^2 \left[{}_{I+1}\beta - {}_I\beta + \frac{1}{2}\{\sin(2_{I+1}\beta) - \sin(2_I\beta)\}\right] \quad \text{for } I = 1, 2, \ldots, N, \\ {}_I\beta_I &= \sin^{-1}\left[\frac{4_IZ^*}{D_2 - D_1}\right] \quad \text{for } I = 1, 2, \ldots, N+1. \end{aligned} \tag{9.2}$$

Next, the reference mean radius $\overline{R}$ of all the disks is specified so that the middle disk has the same inner radius as the actual torus with

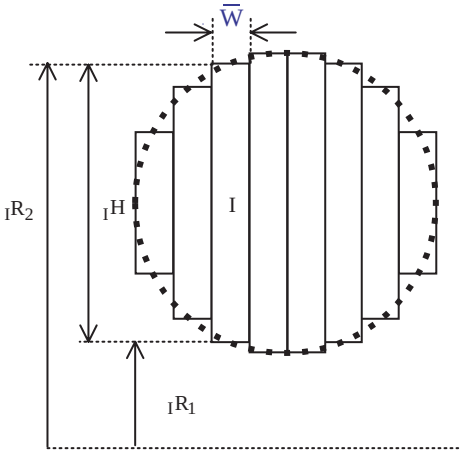

Fig. 6. Approximate model of the circular cross-section of the torus showing the reference geometry of the Ith disk ($N = 8$).

$$\overline{R} = \frac{D_1}{2} + \frac{H_{\max}}{2}, \qquad H_{\max} = \mathrm{Max}({}_I H),$$
$${}_I R_1 = \overline{R} - \frac{{}_I H}{2}, \quad {}_I R_2 = \overline{R} + \frac{{}_I H}{2} \qquad \text{for } I = 1, 2, \ldots, N. \tag{9.3}$$

Using Eqs. (5.4) with a subscript I added to each term, the equilibrium equations associated with the Ith disk can be written in the forms

$$\frac{{}_I w}{2\overline{R}}\, {}_I r_1\, {}_I p_c + \frac{\overline{W}}{3}\frac{\mathrm{d}f}{\mathrm{d}_I \alpha}\left({}_I b - \frac{1}{\lambda^2\, {}_I b^3}\right) = 0, \tag{9.4a}$$

$${}_I \Pi = \frac{1}{3}\frac{\mathrm{d}f}{\mathrm{d}_I \alpha}\left(\lambda - \frac{1}{\lambda_I^3 b^2}\right), \qquad {}_I \alpha = {}_I a^2 + {}_I b^2 + \lambda^2, \tag{9.4b,c}$$

$${}_I a = \frac{1}{\lambda_I b}, \qquad {}_I h = {}_I b_I H, \qquad {}_I w = {}_I a \overline{W}, \qquad \bar{r} = \lambda \overline{R}, \qquad {}_I r_1 = \bar{r} - \frac{{}_I h}{2}, \tag{9.4d–h}$$

$${}_I V_2 = -{}_I V_1 + 2\pi[-{}_I w_I r_{1I} p_c + {}_I H \overline{W}_I \Pi], \tag{9.4i}$$

$${}_I M_2 = -{}_I M_1 + \frac{{}_I w}{2}({}_I V_1 - {}_I V_2), \tag{9.4j}$$

where the external pressure ${}_I p_2$ has been set to zero and the internal pressure ${}_I p_1$ has been denoted as ${}_I p_c$.

For a specified value λ_1 of the stretch of the circumference of the inner portion of the ring, the radius r_1 of this inner portion is given by

$$r_1 = \lambda_1 \frac{D_1}{2}. \tag{9.5}$$

Then, Eqs. (9.4) are solved for the unknowns

$$\lambda, \quad \{{}_I p_c \text{ or } {}_I b\}, \quad {}_I V_1, \quad {}_I V_2, \quad {}_I M_1, \quad {}_I M_2, \tag{9.6}$$

subject to the boundary conditions

$${}_I V_1 = 0, \qquad {}_I M_1 = 0, \qquad {}_{N+1} V_2 = 0, \qquad {}_{N+1} M_2 = 0, \tag{9.7a–d}$$

and the kinematic restriction

$${}_I r_1 \geqslant r_1. \tag{9.8}$$

Also, the kinetic coupling equations

$${}_{I-1} V_2 + {}_I V_1 = 0, \quad {}_{I-1} M_2 + {}_I M_1 = 0 \qquad \text{for } I = 2, 3, \ldots, N, \tag{9.9}$$

require the shear force and moment applied by each disk on its neighbor to be equal in magnitude and opposite in direction.

For a given value of λ_1 these equations are solved iteratively by guessing a value for

$$\lambda. \tag{9.10}$$

Then, from (9.4a,e,g,h) it can be seen that the Ith disk will be free of contact with the cylinder if

$${}_I b = \frac{1}{\sqrt{\lambda}}, \qquad {}_I p_c = 0, \tag{9.11}$$

and the inner radius satisfies the condition

$${}_I r_1 = \lambda \overline{R} - \frac{{}_I H}{2\sqrt{\lambda}} > r_1. \tag{9.12}$$

On the other hand, if (9.12) is not satisfied then the Ith disk is in contact with the rigid cylinder and ${}_Ib$ is determined by the kinematic condition that ${}_Ir_1 = r_1$

$$ {}_Ib = \frac{2}{{}_IH}[\lambda\overline{R} - r_1], \tag{9.13} $$

and the pressure ${}_Ip_c$ is calculated using (9.4a). Next, the values of the shear forces and moments are determined by the conditions (9.4i,j), (9.7a) and (9.9). Then, the value of λ is readjusted until the boundary condition (9.7c) is satisfied. Due to symmetry, the boundary condition (9.7d) will automatically be satisfied by the converged solution.

In order to analyze the results it is convenient to denote $p_{\max}$ as the contact pressure applied to the middle disk, and p_{avg} as the average pressure applied to all disks which are in contact

$$ p_{\text{avg}} = \frac{1}{w_c}\sum_{I=1}^{N} w_I \langle {}_Ip_c\rangle, \qquad w_c = \sum_{I=1}^{N} w_I \mathscr{H}({}_Ip_c), \qquad A_c = 2\pi r_1 w_c, \tag{9.14} $$

where w_c is the length of the edges of the disks which are in contact, A_c is the contact area on the cylinder, $\langle x\rangle$ denotes the McAuley brackets, and $\mathscr{H}(x)$ denotes the Heavyside function

$$ \langle x\rangle = \frac{x + |x|}{2}, \qquad \mathscr{H}(x) = \begin{cases} 1 & \text{for } x > 0, \\ 0 & \text{for } x \leqslant 0. \end{cases} \tag{9.15} $$

Fig. 7 shows the maximum contact pressure $p_{\max}$, the average contact pressure p_{avg} and the axial length w_c of the contact area predicted for two discretizations $N = 1$ and $N = 512$. In order to compare the pressure applied by the ERT device with that applied by standard pressure cuffs the pressure is converted to the units of mm Hg using the conversion factor

$$ 133.3\ \text{Pa} = 1\ \text{mm Hg}. \tag{9.16} $$

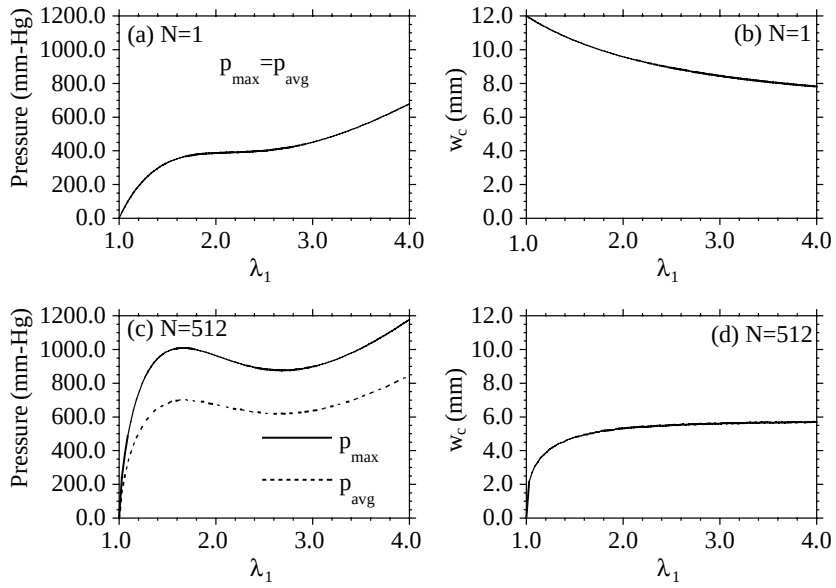

Fig. 7. Response of the approximate Cosserat model of the torus showing the maximum contact pressure $p_{\max}$, the average contact pressure p_{avg}, and the axial length w_c of the contact region versus the stretch λ_1 of the inner radius for $N = 1$ and $N = 512$ rings.

For $N = 1$ the torus is modeled as a single ring with rectangular cross-section. Comparison of the results in Fig. 7a and c shows that this approximation is too crude because the predicted values of the pressure are substantially lower that that for $N = 512$. This means that the models of the previous sections are not able to accurately predict the contact pressure since the extent of the contact region is not modeled correctly (see Fig. 7b and d). When N is greater than unity the prediction of the maximum pressure $p_{\max}$ is a continuous function of the stretch λ_1, but the prediction of the contact length w_c is not continuous as new disks come into contact with the cylinder. For this reason a large value of $N = 512$ was used for Fig. 7c and d so that the curve for p_{avg} will be relatively smooth, but the results are reasonably accurate for much smaller values of N (around $N = 32$).

Fig. 8a shows the deformed shape of the cross-section and Fig. 8b shows the distribution of the contact pressure p_c as functions of the axial coordinate z for $\lambda_1 = 1.5$ and $N = 512$. This value of λ_1 was chosen because from Fig. 7c it can be send that it is close to the value associated with the peak pressure. For this case the deformed disks occupy the region $|z| \leqslant 5.29$ mm but the disks are in contact only in the region $|z| \leqslant 2.39$ mm. In Fig. 8a the radius r_1 of the cylinder has been subtracted from the radial location of the surfaces of the cross-section for convenience. The flat inner surface shown in Fig. 8a is due to contact with the rigid cylinder but the flat outer surface is an unphysical consequence of the constraint that all disks have the same mean radius $\bar{r}$. Moreover, this constraint causes the prediction of the maximum contact pressure $p_{\max}$ to be overestimated by the model. However, it will be shown in the next section that this model

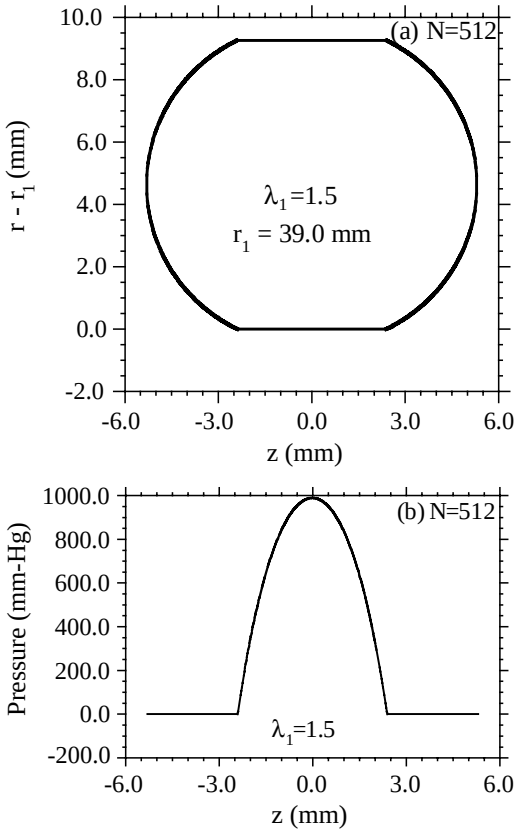

Fig. 8. Plot of: (a) the deformed shape of the cross-section and (b) the axial distribution of the contact pressure p_c for $\lambda_1 = 1.5$ and $N = 512$ using the approximate Cosserat model of the torus.

predicts the average contact pressure p_{avg} much more accurately than the predictions of a single disk (Fig. 7a and b) associated with the previous sections.

10. Finite element calculations

The model of Section 9 is expected to overestimate the maximum contact pressure p_{max} because the shear deformation in each element is constrained to be zero. Since it is important to ensure that the ERT device does not damage tissue it is necessary to evaluate the extent to which the approximate model of Section 9 overestimates the value of p_{max}. To this end, the three-dimensional strain energy function (3.11a) with the specifications (8.3) and (8.5) was implemented in the commercial computer program ABAQUS. Specifically, the strain energy as well as its first and second derivatives were implemented in the subroutine UHYPER which is used to model isotropic elastic response of compressible and incompressible materials. The implementation was verified by a simulation of the uniaxial tensile tests shown in Fig. 5b using the element type CAX6MH which models hybrid axisymmetric elements with 6-nodes and triangular shape.

In order to simulate the deformation of the ring for increasing values of the radius of a rigid cylinder, the following procedure was used: (i) a very stiff thermoelastic cylinder was modeled with axisymmetric elements; (ii) an arbitrary heat expansion coefficient was specified and a homogeneous temperature field was prescribed at the cylinder's nodes; (iii) the value of the temperature was increased in order to increase the radius of the cylinder to obtain the desired stretch λ_1 of the inner surface of the ring. In addition, the ring was prescribed to remain at constant room temperature.

A number of simulations were preformed using friction and hourglass control to verify that the reference calculations (without friction) presented here are properly converged and representative of the expected physical response of the ERT device. Fig. 9 shows the deformed shape of the cross-section and the radial component of the Cauchy stress (mm Hg) for $\lambda_1 = 1.5$. In particular, it can be seen that the Cosserat deformed shape shown in Fig. 8a is reasonably close to that predicted by ABAQUS (Fig. 9) except for the unphysical flat outer region. Fig. 10 compares the predictions of ABAQUS with the approximate Cosserat model ($N = 512$) of Section 9 for: (a) the maximum p_{max} and average p_{avg} contact pressures and (b) the axial length w_c of the line of contact for different values of the internal stretch λ_1. As stated before, the Cosserat

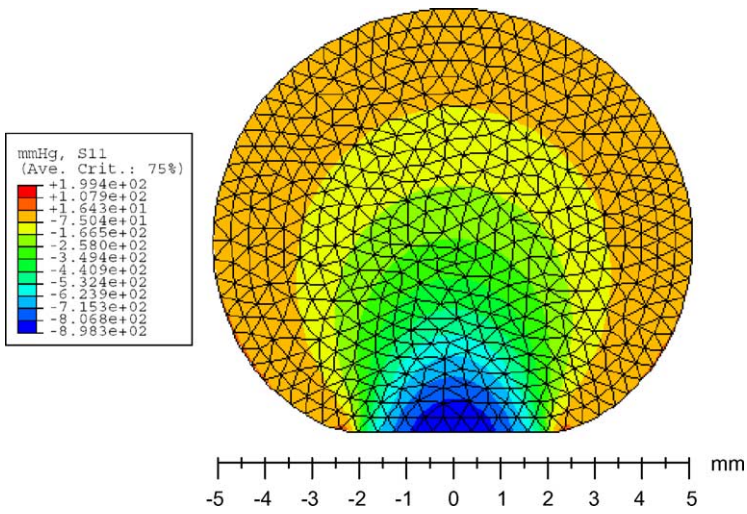

Fig. 9. The deformed shape of the cross-section and the radial component of the Cauchy stress (mm Hg) for $\lambda_1 = 1.5$.

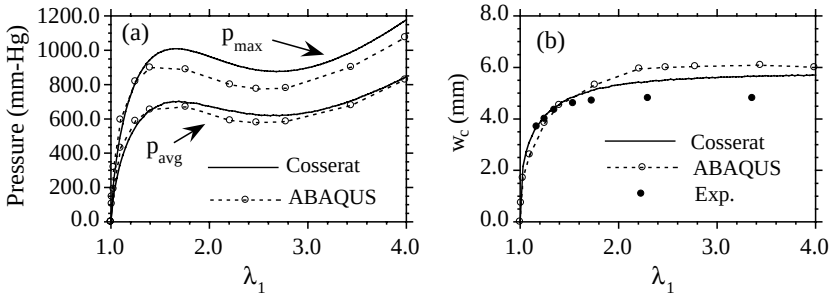

Fig. 10. Comparison of the predictions of ABAQUS and the approximate Cosserat model ($N = 512$) of Section 9 for: (a) the maximum p_{max} and average p_{avg} contact pressures and (b) the axial length w_c of the contact region for different values of the stretch λ_1.

model over predicts the maximum contact pressure but the average contact pressure and the extent of the contact line are surprisingly accurate for such a simple model.

To partially validate the constitutive equation for the silicone ring, experiments were performed to determine the axial length w_c of the contact of the ring with a rigid cylinder. Specifically, the ring was rolled onto cylinders of different radii, the cylinders were sprayed with paint and then the ring was removed and the unpainted region was measured to determine the value of w_c. The experimental results shown in Fig. 10b indicate that the constitutive equation for the ring and the theoretical predictions of w_c are reasonably good for the main range of application ($1.5 \leqslant \lambda_1 \leqslant 2.5$) of the ERT device but that for large values of stretch the theoretical model over predicts the extent of the contact region. This may be partially due to the presence of viscoplasticity in the ring which led to a slightly increased radius of the unloaded ring after being stretched a number of times. Moreover, this viscoplasticity might cause some stress relaxation during more lengthy surgical procedures.

11. Modeling the stockinette

In the actual S-MART™ device some of the stockinette remains rolled on the silicone ring to increase the region of contact with the skin and to reduce the maximum contact pressure. The unstressed radial thickness T_s of the stockinette left on the ring when the S-MART™ device is positioned at the desired location of the limb is easily controlled by adding or removing length form the stockinette during the manufacturing process. Therefore, the value of T_s is an important design parameter which can be used to control the maximum and average pressure applied by the device.

The stockinette is essentially a thin elastic cylindrical tube whose net structure offers only limited resistance to circumferential and axial stretching. Consequently, when it is rolled onto the elastic ring to form the S-MART™ its main effect is to cause an elastic cushion to radial compression of the resulting torus. For this reason the stockinette is modeled as an elastic foundation for the ERT ring. Also, this elastic foundation is assumed to be in uniaxal stress.

To quantify the influence of the stockinette, experiments were performed to determine its uniaxial stress response in compression. Specifically, a few layers of the stockinette, with unstressed thickness $H = 5$ mm, were loaded by different weights with known contact area and the deformed thickness h was measured. This unloaded thickness was chosen because it corresponds to the typical thickness of the stockinette remaining rolled on one model of the S-MART™ device when the tourniquet is placed on the upper portion of the arm. Fig. 11 shows the measured values of the engineering stress Π versus the thickness stretch $\lambda = h/H$. This curve was fitted using an incompressible isotropic hyperelastic material with the strain energy function (5.2) and (8.3) and the material constants specified by

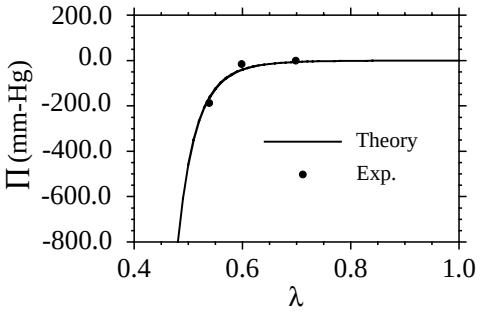

Fig. 11. Measured response of the stockinette for uniaxial engineering stress Π versus thickness stretch $\lambda = h/H$.

$$E_1 = 0, \qquad m = 0, \qquad E_2 = 0.4\,\mathrm{KPa}, \qquad n = 14.0. \tag{11.1}$$

Also, the value of Π was determined by (8.4) and the results are shown in Fig. 11.

The model of Section 9 can be generalized to include the influence of the stockinette by adding an elastic foundation (Fig. 12) to the disks shown in Fig. 6. Specifically, the unstressed radial thickness R_s of the cross-section of the torus associated with the silicone ring and the stockinette is given by

$$R_s = \frac{D_2 - D_1 + 4T_s}{4}. \tag{11.2}$$

Then, using formulas of the type developed in Section 9 which specify that the unstressed cross-sectional area of the model to be the same as that of the torus it can be shown that the unstressed inner radius ${}_IR_0$ of the elastic foundation associated with the Ith stockinette is given by

$${}_IR_0 = \frac{{}_IR_1 + {}_IR_2}{2} - \frac{1}{2\overline{W}}\left[\frac{D_2 - D_1 + 4T_s}{4}\right]^2\left[{}_{I+1}\delta - {}_I\delta + \frac{1}{2}\{\sin(2_{I+1}\delta) - \sin(2_I\delta)\}\right]$$
$$\text{for } I = 1, 2, \ldots, N, \tag{11.3}$$

where the angles ${}_I\delta$ are defined by

$${}_I\delta = \sin^{-1}\left[\frac{4_IZ^*}{D_2 - D_1 + 4T_s}\right] \quad \text{for } I = 1, 2, \ldots, N+1, \tag{11.4}$$

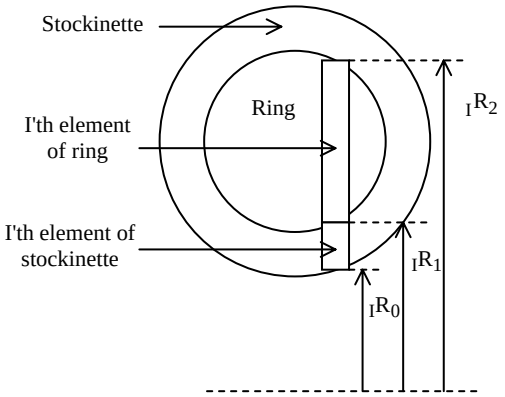

Fig. 12. Sketch of the Ith element of the torus with the model of the stockinette.

and $\{{}_I R_1, {}_I R_2, \overline{W}, {}_I Z^*\}$ are specified by (9.1)–(9.3). Moreover, with the help of (2.5), (8.4) and (11.1) the constitutive equation for the contact pressure ${}_I p_c$ acting in the Ith element is given by

$$ {}_I p_c = -{}_I \lambda_c \Pi_c = -\frac{E_2}{3}\left[\frac{{}_I\lambda_c^3 + 2}{3\,{}_I\lambda_c}\right]^n \qquad \left[{}_I\lambda_c^2 - \frac{1}{{}_I\lambda_c}\right], \qquad {}_I\lambda_c = \frac{{}_I r_1 - {}_I r_0}{{}_I R_1 - {}_I R_0}, \tag{11.5} $$

where ${}_I\lambda_c$ is the stretch of the Ith stockinette element and ${}_I r_0$ is its deformed inner radius.

The modified model of this section is the same as that of Section 9 except that the contact pressure ${}_I p_c$ is now determined by the constitutive equation (11.5) and the kinematic restriction (9.8) is replaced by

$$ {}_I r_0 \geqslant r_1. \tag{11.6} $$

The expression (9.5) is retained for the radius r_1 of the rigid cylinder even though the inner radius of the torus with the stockinette is smaller than the value of r_1 when λ_1 equals unity. For a given value of the inner stretch λ_1 in (9.5) the equations are solved iteratively by first guessing a value for the stretch λ in (9.4). Then, from (9.4a,e,g,h), (11.5) it can be seen that the Ith stockinette will be free of contact with the rigid cylinder if

$$ {}_I b = \frac{1}{\sqrt{\lambda}}, \qquad {}_I p_c = 0, \qquad {}_I\lambda_c = 1, \qquad {}_I r_0 = {}_I r_1 - ({}_I R_1 - {}_I R_0), \tag{11.7} $$

and the inner radius satisfies the condition

$$ {}_I r_0 = \lambda \overline{R} - \frac{{}_I H}{2\sqrt{\lambda}} - ({}_I R_1 - {}_I R_0) > r_1. \tag{11.8} $$

On the other hand, if (11.8) is not satisfied then the Ith stockinette is in contact with the rigid cylinder, ${}_I r_0$ is specified by the kinematic condition

$$ {}_I r_0 = r_1, \tag{11.9} $$

and ${}_I r_1$ are determined iteratively by satisfying the kinetic equations (9.4a) using the constitutive equation (11.5). Next, the values of the shear forces and moments are determined by the conditions (9.4i,j), (9.7a) and (9.9). Then, the value of λ is readjusted until the boundary condition (9.7c) is satisfied. Due to symmetry, the boundary condition (9.7d) will automatically be satisfied by the converged solution. Moreover, it should be emphasized that although it is necessary to solve $N+1$ nonlinear equations for the $N+1$ unknowns

$$ \{\lambda, {}_I r_1\}, \tag{11.10} $$

for a specified value of λ the equations for ${}_I r_1$ are a set of N uncoupled equations so the numerical procedure is relatively efficient. Also, symmetry conditions further reduce the numerical effort.

Since the stockinette is modeled using uniaxial stress elements, the contact pressure between stockinette and silicone ring is equal to the contact pressure between stockinette and rigid cylinder. Fig. 13 shows plots of the maximum pressure (Fig. 13a) and the average pressure (Fig. 13b) for different values of the reference thickness T_s of the stockinette. For $T_s = 0$ the solution is that of Section 9 with $N = 512$ and for the other values of T_s the solution is that of this section with $N = 16$. This solution for the maximum pressure for $N = 16$ is converged since it is quite close to the solution for $N = 8$. Some oscillations occurred in the solution for the average pressure with $T_s = 2$ mm and are due to the discreteness of the mesh which causes discontinuities in the contact area as a new element comes into contact.

Most importantly, it can be observed from Fig. 13a that increasing the thickness T_s of the stockinette can significantly reduce the magnitude of the maximum contact pressure. Also, it can be seen from Fig. 13b that for the cases with the stockinette, the average pressure is nearly insensitive to the value of T_s and that its value in the typical range of application of the ERT (about $1.5 \leqslant \lambda_1 \leqslant 2.5$) is about 400 mm Hg. The calculated average pressure is considerably reduced with respect to the calculations without stockinette. This

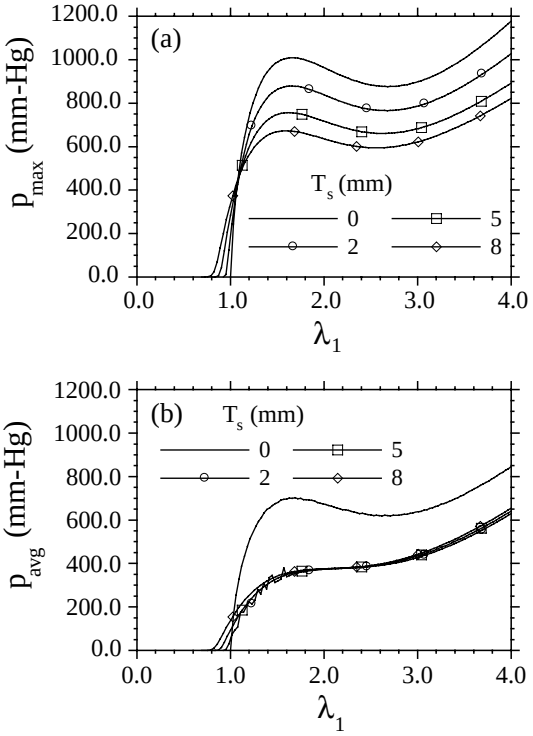

Fig. 13. Plots of: (a) the maximum contact pressure and (b) the average contact pressure versus the stretch λ_1 for different values of the reference thickness T_s of the stockinette.

reduction is due to an increase of the contact area which might be overestimated by the present model since some radial support is provided by stockinette in elements at the extremities of the contact region, where the normal to the actual ring has a larger axial component than radial component.

Fig. 14 shows the results of calculations for a rigid cylinder of radius 39 mm (corresponding to a stretch $\lambda_1 = 1.5$). Specifically, Fig. 14a shows the deformed shape of the cross-section of the silicone ring for $T_s = 5$ mm, and Fig. 14b shows the axial distribution of the contact pressure p_c for different values of T_s. The space below the ring in Fig. 14a is supported by the compressed stockinette. The results in Fig. 14b for $T_s = 0$ are those of Section 9 with $N = 512$, whereas the other results are those of this section with $N = 128$. This high value of N was used to produce smooth pressure distributions, but as noted earlier the solution converges for values of N around 16. Again, it can be seen from Fig. 14b that the thickness T_s of the stockinette has a significant influence on the peak values of the contact pressure.

A finite element mesh was developed to model the stockinette as a cylindrical shell of reference radial thickness 5 mm and axial length 20 mm, which was placed in sliding contact with the outer surface of a rigid cylinder of radius 39 mm (corresponding to $\lambda_1 = 1.5$). Initially, the stockinette shell was prestretched slightly to simulate its state when rolled on the ring. This finite element simulation of the ERT device is not straight forward. In several attempts the calculations failed to converge. The difficulties are mainly related to the fact that the problem investigated is characterized by two sources of nonlinearity: the nonlinear material behavior (especially of the stockinette) and the opening and closing of contact surfaces at the ring-stockinette and stockinette-cylinder interfaces. Convergence problems were solved by adjusting the mesh refinement at these contact interfaces, with smaller elements used for the so called "slave surface" (corresponding to the softer stockinette material) with respect to the "master surface".

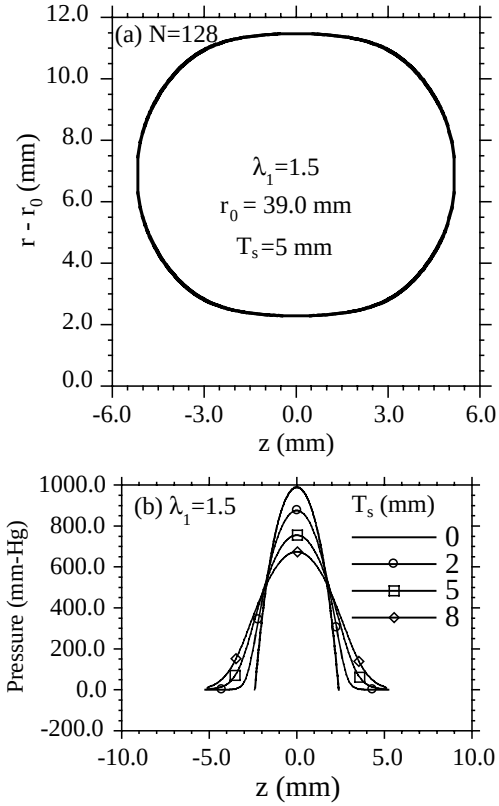

Fig. 14. Plots of: (a) the deformed shape of the cross-section for $T_s = 5$ mm and (b) the axial distribution of the contact pressure p_c for different values of T_s. $\lambda_1 = 1.5$ and $N = 128$.

In the simulations, the silicone ring was stretched by external radial forces and placed over the stockinette. Finally, these external radial forces were progressively removed and the structure was relaxed to equilibrium. In spite of these special efforts, repeated opening and closing of the contacts at specific nodes during the calculations led to so called "severe discontinuity iterations", which in turn resulted in cutbacks of the time increments. As a consequence, a large number of increments with multiple iterations had to be calculated, so the calculation times were about 10 min for one single value of stretch λ_1 (one equilibrium state) with the present hardware implementation. This should be compared with a calculation time of about 10 min using the Cosserat theory for simulating the 100 equilibrium states in each of the curves shown in Fig. 13. Thus, simulations using the Cosserat model are characterized by considerably smaller calculation times than those for the proposed finite element model. In addition, the Cosserat model is more suitable for optimization purposes, since different values of the stockinette thickness T_s can be simulated by changing one single input parameter of the calculation. In contrast, for the finite element model a new mesh has to be created for each thickness value, which is a time consuming process for the user rather than for the computer.

Fig. 15 shows the deformed configuration of the stockinette and the silicone ring and the radial component of the Cauchy stress for a rigid cylinder with $\lambda_1 = 1.5$. Comparison of the results in Fig. 14a and Fig. 15 shows that Cosserat and finite element models predict similar shapes and sizes of the cross-section of the silicone ring for a stockinette of reference thickness $T_s = 5$ mm. Also, the value $p_c = 755$ mm Hg of the

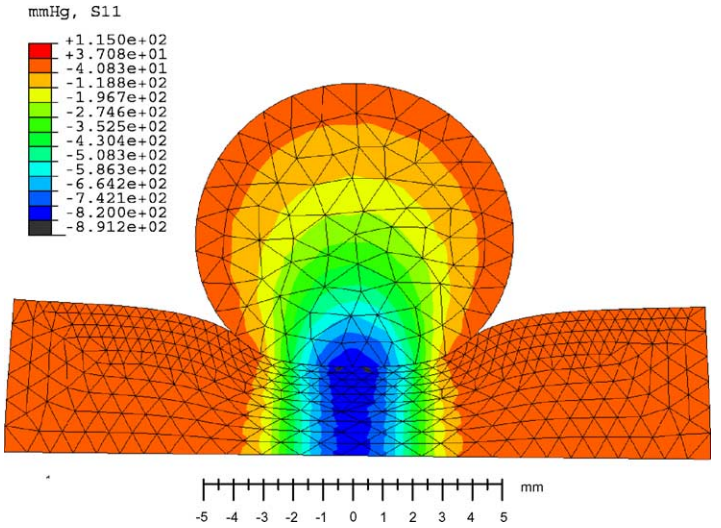

Fig. 15. Deformed configuration of the stockinette and the silicone ring and the radial component of the Cauchy stress for a rigid cylinder with $\lambda_1 = 1.5$.

maximum contact pressure predicted by the Cosserat model is reasonably close to the value $p_c = 790$ mm Hg of the maximum contact pressure between stockinette and rigid cylinder predicted by the finite element model. The difference between these two values is mainly due to the fact that the axisymmetric finite element model admits circumferential stresses in the stockinette which have magnitudes about 60% of the radial stresses. This effect stiffens the stockinette and causes its radial thickness to be larger than that predicted by the Cosserat model. Moreover, it can be seen from Fig. 15 that the radial stress in the stockinette in nearly uniform axially which partially justifies the assumption of an elastic foundation in the Cosserat model.

12. Conclusions

Here, it has been shown that accurate determination of the contact pressure applied by a silicone ring model of the ERT device is surprisingly difficult. In particular, the analysis necessarily must include: cross-sectional deformations, the specific shape of the cross-section of the ring, large deformations, the influence of contact pressures which are of the same order as the circumferential stresses, and material nonlinearity. Since the effects of bending are insignificant the Cosserat theory of a generalized string (which includes deformation of the cross-section) provides a sufficiently accurate model of the ring that can easily incorporate nonlinear material properties.

A special constrained Cosserat theory of a generalized string was developed to model details of the toroidal shape of the ERT device and the predictions of the contact pressure and the axial extent of the contact region have been shown to be in reasonable agreement with axisymmetric finite element analysis using the program ABAQUS. In addition, more detailed Cosserat and finite element models have been used to show the significant influence of the stockinette sterile gauze in the S-MART™ device on the reduction of both the maximum and average contact pressures. Since numerical simulations with the Cosserat model are considerably faster than those with the finite element models, the Cosserat analysis is more suitable for optimization of the thickness of the stockinette.

Acknowledgments

This research was partially supported by the fund for promotion of research at the Technion. Also, M.B. Rubin would like to thank Dr. N. Gavrieli, O. Gavrieli, and R. Levenson from OHK Medical Devices for helpful discussions and for providing some of the experimental data.

References

Antman, S.S., 1972. The theory of rods. In: Truesdell, C. (Ed.), S. Flugge's Handbuch der Physik, vol. VIa/2. Springer-Verlag, Berlin, pp. 641–703.

Antman, S.S., 1995. Nonlinear problems in elasticity. Applied Mathematical Sciences, vol. 107. Springer-Verlag, Berlin.

Boiko, M., Roffman, M., 2004. Evaluation of a novel tourniquet device for bloodless surgery of the hand. J. Hand Surg. B 29, 185–187.

Green, A.E., Naghdi, P.M., Wenner, M.L., 1974a. On the theory of rods—Part I: Derivations from the three-dimensional equations. Proc. R Soc. London A 337, 451–483.

Green, A.E., Naghdi, P.M., Wenner, M.L., 1974b. On the theory of rods—Part II: Developments by direct approach. Proc. R Soc. London A 337, 485–507.

Naghdi, P.M., Rubin, M.B., 1989. On the significance of normal cross-sectional extension in beam theory with application to contact problems. Int. J. Solids Struct. 25, 249–265.

OHK Medical Devices, 2002. Division of Oneg HaKarmel Ltd, Haifa, Israel, <www.ohkmed.com>.

Paris-Seeley, N.J., McEwen, J.A., Romilly, D.P., 2000. A compliance-independent pressure transducer for biomedical device-tissue interfaces. Biomed. Instrum. Technol. 34, 423–431.

Rivlin, R.S., 1949. Large elastic deformations of isotropic materials. VI. Further results in the theory of torsion, shear and flexure. Phil. Trans. R Soc. London A 242, 173–195.

Rubin, M.B., 1996. Restrictions on nonlinear constitutive equations for elastic rods. J. Elasticity 44, 9–36.

Rubin, M.B., 2000. Cosserat theories: shells, rods and points. Solid Mechanics and its Applications, vol. 79. Kluwer, The Netherlands.